Percolation phenomena of calcium bis(2-ethylhexyl) sulfosuccinate water - in - oil microemulsions by dielectric spectroscopy

Percolation phenomenon of calcium bis(2-ethylhexyl) sulfosuccinate water-in-oil microemulsions by conductivity and dielectric spectroscopy measurements

Giulia Capuzzi and Piero Baglioni
Department of Chemistry and CSGI, University of Florence, 50121 Florence, Italy

Cecilia M. C. Gambi
Department of Physics, University of Florence and INFM, Largo Enrico Fermi 2, 50125 Florence, Italy

Eric Y. Sheu
Vanton Research Laboratory, P.O. Box 572, Hopewell Junction, New York 12533
(Received 23 July 1998; revised manuscript received 11 January 1999)

The sodium counterion (Na^+) of the sodium bis(2-ethylhexyl) sulfosuccinate (AOT) surfactant was exchanged with calcium Ca^{2+} to investigate the counterion charge effect on the structure of water in normal decane microemulsions. Ohmic conductivity and dielectric permittivity measurements were performed on samples at constant water to surfactant mole ratio [water]/[$Ca(AOT)_2$]=26.6. Increasing the volume fraction of the dispersed phase ϕ, a percolation phenomenon was observed at the constant temperature of 25° C. The percolation threshold was found at $\phi \sim 15\%$ by Ohmic conductivity and static dielectric permittivity studied as a function of ϕ, and by the frequency dependence of the complex permittivity. Critical exponents typical of the static percolation mechanism (formation of bicontinuous microemulsions) were found below and above threshold. The comparison of these results obtained for the two different counterions, Ca^{2+} and Na^+, in AOT surfactant water in normal decane microemulsions allows detection of an important difference. The percolation below threshold is dynamic for the sodium-based microemulsions, accounting for the formation of clusters of droplets, whereas calcium-based microemulsions show a static percolation. For this system, the coalescence of droplets begins to occur below threshold at $\phi \sim 12\%$. [S1063-651X(99)12807-1]

PACS number(s): 61.25.Hq, 64.70.Ja, 77.22.−d, 82.70.Dd

I. INTRODUCTION

Counterion-induced effects are important either in fundamental or in applied research [1–8]. Substitution of a monovalent with a divalent counterion, in a surfactant molecule of self-assembled structures, can produce a consistent change of the surfactant solubility in water, of the aqueous critical micellar concentration, and of the phase diagram. To clarify the role of the counterion charge variation, we present a study of self-assembled aggregates formed by surfactant with divalent calcium counterion and we compare the results with the monovalent, sodium reference system. The calcium ions are very important in biological processes such as calcium adsorption at the cell membranes [9] in pharmaceutical and food technology [10].

In this paper we focus our attention on the substitution of sodium with calcium in the sodium bis(2-ethylhexyl) sulfosuccinate [Na(AOT)] water in normal decane microemulsions. The Na(AOT) water in *n*-decane microemulsions reference system was chosen because the structure of these microemulsions is well known by means of different experimental techniques [11–21]. The phase diagram of the $Ca(AOT)_2$ water in *n*-decane microemulsion system and preliminary small-angle neutron scattering (SANS) results [8] evidenced analogies and differences between the calcium AOT and the sodium AOT microemulsions. For example, the extension of the microemulsion monophasic domain is significantly reduced for the calcium-based system. Furthermore, a SANS study of the dilute region of the phase diagram showed the presence of smaller droplets formed with the calcium AOT surfactant [8]. A few other calcium AOT ternary microemulsions, $Ca(AOT)_2$-water-cyclohexane and $Ca(AOT)_2$-water-isooctane, have been investigated at very low water to surfactant ratio of ≤ 5 [1–4]. These microemulsion systems are formed by spherical droplets in the isotropic $L2$ phase.

To have an insight into the evolution of the system structure in the concentrated region of the phase diagram, we investigate, via dielectric spectroscopy and conductivity measurements, the calcium AOT water in *n*-decane microemulsions. In fact, working at a suitable water to surfactant ratio and increasing the volume fraction of the dispersed phase ϕ (defined as ratio of water plus surfactant over total), the microemulsion evolves continuously from transparent homogeneous fluid samples to transparent viscous homogeneous samples as many other water-in-oil microemulsions for which the conductivity and dielectric spectroscopy investigation, in addition to other techniques, clarified the structural evolution [11–30].

A preliminary analysis by conductivity and dielectric spectroscopy measurements showed that a percolation phenomenon occurs. A water to surfactant mole ratio of 26.6 was chosen to detect the percolation threshold and to analyze the phenomenon. When a percolation phenomenon occurs in microemulsions, a dynamic or a static percolation can be identified [31–35], corresponding, respectively, to the formation of clusters of droplets or to the coalescence of the droplets into water channels (bicontinuous structures). In the dilute region, the electrical conduction mechanism is interpreted in terms of the droplet charge fluctuations model

[36–38], i.e., the droplets, on the average electrically neutral, can carry excess charge due to spontaneous thermal fluctuations of composition, and migrate in an electric field. Moreover, the permittivity values can be calculated in term of the Hanai's model [39,40] which takes into account the interfacial polarization mechanism described by the Maxwell-Wagner theory. Approaching the percolation threshold, either by increasing the temperature or the number density of droplets or pressure, coalescence can occur leading to bicontinuous microemulsions (static percolation). In other cases the hopping of surfactant molecules and/or counterions, or portions of interfacial regions that occurs mediated by diffusional approach and separation of the droplets produces the percolation process (dynamic percolation). In both dynamic and static regimes the static dielectric permittivity diverges and the Ohmic conductivity shows a steep increase. At threshold, at least one cluster of droplets (or one water channel) connects the system from one electrode to the other. A further increase of the parameter chosen to observe the percolation phenomenon will produce an increase in the number of clusters or bicontinuous channels for dynamic and static percolation, respectively. In both cases, the trend of the Ohmic conductivity and static permittivity are similar; the difference between the two physical processes being detectable only by studying the scaling laws.

In this paper, the percolation phenomenon of calcium AOT water in *n*-decane microemulsions is studied at a constant temperature of 25° C. The results are compared with those of the sodium AOT water in *n*-decane microemulsions to have an insight into the role of counterion charge on the microemulsion structure.

II. THEORETICAL MODEL

It is generally assumed that a water-in-oil microemulsion is made of two components, a dispersed water phase (1) and a continuous oil phase (2); thus the complex permittivity ϵ^* is a function of the complex permittivities of the dispersed phase ϵ_1^* and of the continuous phase ϵ_2^*, where $\epsilon_i^* = \epsilon_{is} - j\sigma_i/(\omega\epsilon_o)$ for $i=1,2$. The two components are dielectric conductors of static permittivity ϵ_{1s} and ϵ_{2s} and conductivity σ_1 and σ_2; ϵ_o is the permittivity of vacuum, $\omega = 2\pi \cdot f$, f is the frequency, and $j^2 = -1$. The *n*-decane conductivity is close to zero and its static dielectric constant is 1.99. Water and *n*-decane do not show dielectric adsorption in the frequency range investigated; thus $|\epsilon_1^*| \gg |\epsilon_2^*|$, and the general relationship for the microemulsion complex permittivity ϵ^* is [23]

$$\frac{\epsilon^*}{\epsilon_1^*} = |\phi - \phi_p|^{\mu} f\left(\frac{\epsilon_2^*/\epsilon_1^*}{|\phi - \phi_p|^{(\mu+s)}}\right), \tag{1}$$

where ϕ_p is the concentration at the percolation threshold and μ and s (both greater than zero) are the percolation exponents. Except in the neighboring of ϕ_p, where the argument of the function f diverges, f satisfies the following asymptotic forms [23]:

$$\phi > \phi_p, |z| \ll 1, f(z) = c_1 + c_2' z, \tag{2a}$$

$$\phi < \phi_p, |z| \ll 1, f(z) = c_2 z, \tag{2b}$$

$$|z| \gg 1, f(z) = c z^{\mu/(\mu+s)}, \tag{2c}$$

for each ϕ value. In our case, $\epsilon_{1s} \sim 80$ and $\epsilon_{2s} \sim 2$ are constant values up to 13 MHz, upper frequency studied. This implies that z is a positive real value lower than 1, and the asymptotic laws are

$$\epsilon_s = c_2 \epsilon_{2s} (\phi_p - \phi)^{-s}, \tag{3}$$

$$\sigma = c_2 \sigma_2 (\phi_p - \phi)^{-s}, \tag{4}$$

below the percolation threshold, and

$$\epsilon_s = c_1' \epsilon_{2s} (\phi - \phi_p)^{-s} + c_1 \epsilon_{1s} (\phi - \phi_p)^{\mu}, \tag{5}$$

$$\sigma = c_1' \sigma_2 (\phi - \phi_p)^{-s} + c_1 \sigma_1 (\phi - \phi_p)^{\mu}, \tag{6}$$

above the percolation threshold. c_1, c_1', and c_2 are constants. Below threshold, $\epsilon_s(\phi)$ and $\sigma(\phi)$ [Eqs. (3) and (4)] show a simple exponential law with a single exponent s. Above threshold, as $\epsilon_{2s}/\epsilon_{1s} \sim 1/40$, Eq. (5) can show different trends depending on c_1' and c_1 values. In Eq. (6), because $\sigma_2 \ll \sigma_1$, we reasonably expect a $\sigma(\phi)$ dependence above threshold described by an exponential law with single exponential:

$$\sigma = c_1 \sigma_1 (\phi_p - \phi)^{\mu}. \tag{7}$$

The conductivity and the static dielectric constant scaling laws are characterized by the two critical exponents μ and s. The μ exponent is in the range from 1.5 to 2 for both static and dynamic percolation, whereas $s = 0.6$ to 0.7 for static and $s \sim 1.2$ for dynamic percolation [31,32].

To describe the frequency dependence of the microemulsion complex permittivity at percolation, we recall that a theory on random resistor networks near their percolation threshold [41] was modified to describe quite well some microemulsions at percolation [27]. For the conductor-insulator mixture, the frequency dependence of the complex permittivity takes the form:

$$\epsilon^*(\omega) = E \omega^{u-1} \exp[j\pi(1-u)/2], \tag{8}$$

where E is real, $\omega = 2\pi f$, where f is the linear frequency, and u is a critical exponent. Equation (8) implies that both the real and the imaginary parts of ϵ^*, $\epsilon'(\omega)$ and $\epsilon''(\omega)$, respectively, exhibit a ω^{u-1} frequency dependence and that the loss angle Δ defined by $\tan\Delta(\omega) = \epsilon''(\omega)/\epsilon'(\omega)$ is independent of frequency and equal to $\pi(1-u)/2$, close to percolation threshold. Furthermore, the exponent u is related to μ and s by the equation $u = \mu/(\mu+s)$. Values of u between 0.56 and 0.63 are expected for dynamic percolation, and between 0.68 and 0.77 for static percolation. These values lead to loss angle tangent values of 0.69 to 0.58 and of 0.50 to 0.36 for dynamic and static percolation, respectively. As the microemulsion differs from the conductor-insulator mixture, the above considerations related to conductor-insulator mixtures apply, in microemulsions, in a frequency range that is characteristic of the microemulsion system investigated [27].

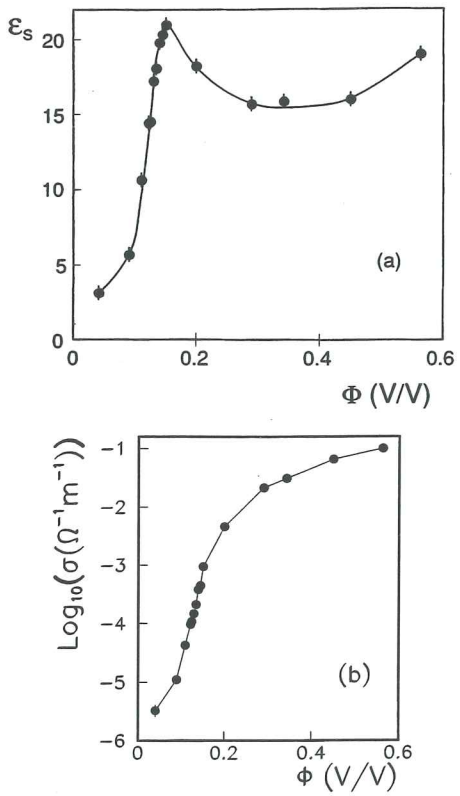

FIG. 1. Experimental static dielectric constant (a) and Ohmic conductivity (b) as a function of the volume fraction of the dispersed phase, for $Ca(AOT)_2$ water in *n*-decane microemulsion samples along the dilution line [water]/[surfactant]=26.6 at $T=25\,^{\circ}C$. The lines are a guide for the eyes.

III. EXPERIMENT

The calcium salt of AOT was prepared by aqueous metathesis of a saturated solution of $Ca(NO_3)_2$ (Aldrich AR) with an ethanolic solution of Na(AOT) (Sigma). The $Ca(AOT)_2$ precipitate was separated from the aqueous phase by settling, and washed repeatedly with Millipore grade water until complete disappearance of NO_3^- (determined by the brown ring test) and Na^+ ions (atomic adsorption spectroscopy). The remaining water was eliminated by freeze drying. *N*-decane was from Fluka AG (purum>99%, olefin free) and water was from Millipore, Milli-Q system. All the samples studied were prepared by diluting with *n*-decane a stock solution at constant water to surfactant mole ratio of 26.6. The temperature was kept constant at $25.0\pm0.05\,^{\circ}C$ by a thermostatic bath.

The conductivity and dielectric spectroscopy measurements were performed with a Hewlett Packard 4192A low-frequency impedance analyzer (frequency range 5 Hz to 13 MHz). The cell was a four-terminal sample holder device with parallel, rectangular gold plate electrodes having the surfaces roughened to minimize electrodes polarization (see Fig. 1 reported in Ref. [42] where the cell is described in details).

The cell filled with the microemulsion sample can be represented by an equivalent parallel resistance-capacitance electrical circuit with the resistance R and the capacitance C given by

$$R=1/(\omega k\epsilon_o\epsilon''+k\sigma),\quad C=k\epsilon_o\epsilon', \tag{9}$$

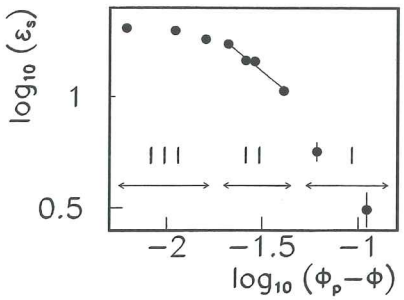

FIG. 2. Experimental values $\epsilon_s(\phi)$ for $\phi<0.145$ in double logarithmic scale. Three different concentration regions, corresponding to different physical processes, are shown. I—for $\phi<0.090$ the process is not percolative and can be interpreted in terms of the Hanai model. II—for $0.090<\phi<0.130$ the experimental values follow, according to the scaling law [Eq. (3)], a linear trend of $\log_{10}(\epsilon_s)$ vs $\log_{10}(\phi_p-\phi)$ from which the critical exponent of the percolative process is calculated. III—for $0.130<\phi<0.145$ the experimental values are close to the percolation threshold where the f function of Eq. (1) diverges.

where ϵ_o is the permittivity of free space, $\epsilon'-j\epsilon''$ is the complex permittivity of the medium ($j^2=-1$), σ is the Ohmic conductivity of the sample, and k is the cell constant depending on the cell geometry. In a real cell, other contributions are present: for the cell used, a stray capacitance C_o in parallel to the RC circuit, a series resistance R_s, and a series self-inductance L_s. The parameters k, C_o, R_s, and L_s were evaluated by the calibration procedure described in [42]. To evaluate R and C, as a first step, the sample Ohmic conductivity is measured in a low-frequency range in which the electrode polarization does not affect the measurements. Then the frequency dependence of the impedance magnitude and phase angle of the dielectric cell is detected. To extract the complex permittivity values, the electrical circuit described above (see Fig. 2 of [42]) was used to evaluate R and C as a function of the measured parameters. As shown in Eq. (9), R is representative of the sample Ohmic resistance and of the dielectric adsorption; thus, ϵ'' is extracted from R, after subtraction of the Ohmic conductivity already measured. From C, ϵ' is obtained.

IV. RESULTS

In Fig. 1, the Ohmic conductivity and the static dielectric constant at $25\,^{\circ}C$ are shown as a function of the volume fraction of the dispersed phase ϕ. The explored ϕ range is 0.041 to 0.563. Throughout the paper, the error bars are standard deviations. When the errors do not appear on the figure, they are smaller than the symbols used. From the behavior of the static permittivity $\epsilon_s(\phi)$ and conductivity $\sigma(\phi)$ curves two different regions can be identified. In the dilute region ($\phi<0.10$), the ϵ_s and σ values are low. At $\phi>0.10$, ϵ_s and σ increase rapidly as a function of ϕ and show percolative trends.

In the dilute region, the conductivity data can be analyzed by the droplets charge-fluctuation model [36–38], assuming a model of hard spheres of radius 26.5 Å . This value was obtained from SANS investigation [8] for the $Ca(AOT)_2$-water-deuterated normal decane system. For this system, the SANS experiment detects, due to the particular

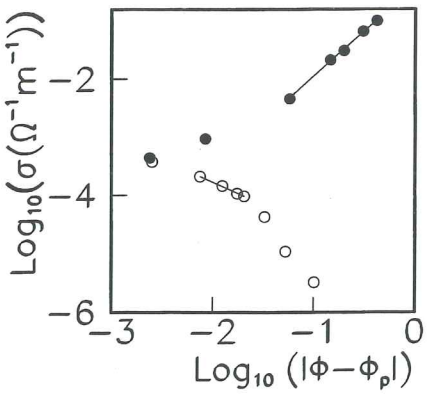

FIG. 3. Experimental values $\sigma(\phi)$ in double logarithmic scale. The plot shows the data below (open circles, bottom curve) and above (full circles, upper curve) the percolation threshold $\phi_p = 0.142$. The straight lines represent the fitting results [see Eqs. (4) and (7)]. For $\phi < 0.110$ the nonpercolative behavior is described by the charge-fluctuation model. Close to the percolation threshold the scaling laws do not apply as the f function of Eq. (1) diverges.

contrast chosen, the particle core and its interfacial region, whose sum is close to the hydrodynamic particle radius, which must be used in the application of the charge-fluctuation model. The experimental data follow this model up to $\phi \sim 0.09$. In the same concentration range, the static dielectric constant agrees with the Hanai model [39,40], which considers the system composed by hard spheres of water plus surfactant dispersed in the continuous oily matrix.

For $\phi > 0.10$, the hard-sphere model does not apply and percolation must be invoked to justify the observed conductivity and permittivity trends. In Fig. 1, as ϕ approaches the percolation threshold, the static dielectric constant exhibits a maximum followed by a broad minimum and a slight $\epsilon_s(\phi)$ increase at high ϕ. A percolation threshold at $\phi_p = 0.151 \pm 0.004$, can be estimated by the position of the maximum. The errors evaluated are standard deviations throughout the paper. The $\sigma(\phi)$ curve is characterized by a typical sigmoidal shape with a sharp increase near the percolation threshold. The percolation threshold $\phi_p = 0.142 \pm 0.002$ was obtained from the analysis of the curvature variation of the $\sigma(\phi)$ curve. In the limit of the experimental errors, the conductivity and the dielectric percolation thresholds are similar. The analysis of the $\epsilon_s(\phi)$ curves for the samples below the

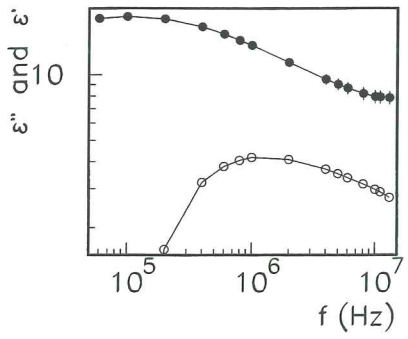

FIG. 4. The real and the imaginary parts of the dielectric complex permittivity (ϵ', full circles and ϵ'', open circles) are reported versus frequency, for the sample with $\phi = 0.135$, at $T = 25\,^{\circ}\mathrm{C}$. The continuous lines are a guide for the eyes.

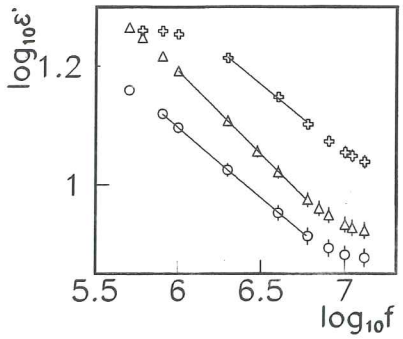

FIG. 5. The $\log_{10}(\epsilon')$ versus $\log_{10}(f)$ curves are shown for samples with $\phi = 0.130$ (open circles), 0.145 (open triangles), and 0.200 (open crosses). The straight lines represent the fitting results [see Eq. (8)].

percolation threshold was performed according to Eq. (3). The experimental data are plotted in Fig. 2 in double logarithmic scale. A linear trend is shown in the concentration range from 0.110 to 0.130. From the slope of the straight line the exponent $s = 0.69 \pm 0.09$ can be obtained. We recall that a dynamic percolation process is characterized by a critical exponent $s \sim 1.2$, whereas the coefficient for static percolation processes is $s \sim 0.7$. Therefore, the s value supports a static percolation mechanism. In the $\epsilon_s(\phi)$ curve, the scaling exponents above threshold cannot be evaluated for the reasons summarized in Sec. II. The analysis of the $\sigma(\phi)$ data (see Fig. 1), in terms of the scaling laws [Eqs. (4) and (7)] is reported in Fig. 3. The critical exponents obtained from the linear behavior of the curves in double logarithmic scale are $s = 0.78 \pm 0.03$ and $\mu = 1.542 \pm 0.014$, respectively, below and above the percolation threshold, confirming the static model. The linear trend below threshold extends from 0.122 to 0.135, a range similar to that for the static permittivity. Above threshold it extends from 0.200 to 0.563.

The frequency dependence of the dielectric permittivity was also analyzed. As an example, the frequency dependence of both the real and the imaginary parts of the complex permittivity are reported in Fig. 4 for the sample with the volume fraction of the dispersed phase $\phi = 0.135$. Typical trends of percolation in microemulsions are shown by the ϵ' and ϵ'' curves. The frequency of the maximum absorption is at ~ 1 MHz, a value typical of microemulsions. The dielectric spectrum of Fig. 4 shows a rather broad dispersion; futhermore,

TABLE I. The critical exponent u and the maxima values of $\tan\Delta$ for samples at [water]/[surfactant] = 26.6.

ϕ	u	$\tan\Delta_{max}$
0.110		0.20±0.01
0.122		0.32±0.01
0.125		0.34±0.01
0.130	0.77±0.01	0.37±0.01
0.135	0.76±0.01	0.39±0.01
0.140	0.74±0.01	0.42±0.01
0.145	0.73±0.01	0.43±0.01
0.151	0.78±0.01	0.44±0.01
0.200	0.77±0.01	0.38±0.01

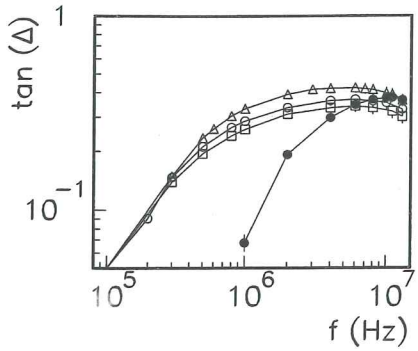

FIG. 6. The tan Δ versus frequency for the samples with ϕ = 0.125 (open squares), 0.130 (open circles), 0.145 (open triangles), and 0.200 (full circles). The continuous lines are a guide for the eyes. Broad maxima are shown by most of the curves in a frequency range intermediate between 1 MHz and 10 MHz where tan(Δ) is almost independent on frequency. The curve with full points (ϕ=0.200) does not show a maximum as the frequency range is too narrow.

the $\epsilon''(f)$ curve is strongly asymmetric as other cases reported in the literature [19,27,43]. In [19], the presence of a broad dispersion and the asymmetry of the dispersion, which indicate a distribution of relaxation times, are fully discussed in both frequency and time domains. In this paper, we perform the analysis in the frequency domain following the procedure previously described in Sec. II. The ϵ' versus frequency curves show a linear trend in double logarithmic scale for the samples with $0.11<\phi<0.29$. In Fig. 5 three representative curves are shown in the frequency range where the critical exponent u was calculated. For all the samples studied, the u values are reported in Table I. All the values calculated are typical of static percolation. We performed the data analysis also at ϕ = 0.110, 0.122, and 0.125 (not reported in Table I) but the calculated exponents are higher than those expected for both static and dynamic percolation, indicating that in this case the investigated concentrations are too far from the percolative threshold. At $0.200 < \phi \leq 0.290$, the frequency range investigated is too narrow to analyze the curve.

As reported in Sec. II, the loss angle Δ defined by $\tan\Delta(\omega)=\epsilon''(\omega)/\epsilon'(\omega)$ is independent of frequency and equal to $\pi(1-u)/2$, close to percolation threshold. Figure 6 shows the $\tan\Delta(f)$ curves for some samples studied. All the samples studied show a frequency-independent range in the $\tan\Delta(f)$ curve where $\tan\Delta$ reaches a maximum. These maxima values are reported in Table I. At concentration of ϕ = 0.110, the maximum is very broad and the value is lower than that of both static and dynamic percolation. Increasing ϕ, the maxima increase towards values typical of static percolation, up to the highest value, $\tan\Delta=0.44$, at ϕ = 0.151. A further increase of ϕ leads to a decrease of the maximum value. At $\phi \geq 0.200$, $\tan\Delta(f)$ increases as the frequency increases because the frequency range is too narrow to analyze the curve. Thus, no sample reaches a value typical of dynamic percolation.

From the analysis of conductivity and static permittivity as a function of the volume fraction of the dispersed phase, a percolation threshold ϕ_p around 0.15 was found. The frequency analysis gives the highest $\tan\Delta$ vs frequency values at $\phi \sim 0.15$ (see Table I). We point out that the frequency dependence confirms the description of the percolation phenomenon in term of the static model (bicontinuous microemulsions). Thus, bicontinuous water channels in oil begin to form in the system starting at $\phi \sim 12\%$.

V. DISCUSSION AND CONCLUSION

In this paper, Ohmic conductivity and dielectric permittivity were measured on samples of $Ca(AOT)_2$ water in *n*-decane microemulsions with $[water]/[Ca(AOT)_2]=26.6$. After a preliminary investigation, the water to surfactant mole ratio 26.6 was chosen to perform the numerical analysis below and above threshold. The results clearly show that percolation occurs in calcium AOT water in *n*-decane microemulsions. A threshold of ~15% of volume fraction of the dispersed phase was found by Ohmic conductivity and static dielectric constant as a function of ϕ and by frequency variation of the complex permittivity. The percolation mechanism is static both below and above the percolation threshold. In fact, an exponent $s \sim 0.7$ was calculated by the $\sigma(\phi)$ and $\epsilon_s(\phi)$ scaling behaviors. Furthermore, by the complex permittivity frequency dependence, the exponent u is between 0.73 and 0.78, in a large ϕ interval around threshold 0.13 to 0.20. In the same ϕ interval the $\tan\Delta$ vs frequency has a maximum that spans from 0.37 to 0.44. These values are typical of the static percolation phenomenon. Therefore, the conductivity and the dielectric permittivity characterization strongly suggests that the $Ca(AOT)_2$ water in n-decane microemulsions form water channels in oil, starting from ϕ values of ~12%. Further work is in progress to study the structural evolution by small-angle neutron scattering, in order to understand how almost spherical droplets, found by SANS [8] at $\phi<10\%$, evolve towards elongated water channels. In [44], viscosity, conductivity, dynamic light scattering, and NMR self-diffusion measurements were performed to have a preliminary insight into the calcium AOT water in *n*-decane microemulsion. The results indicate a preference of the system to form bicontinuous microemulsions. We have to point out that the conductivity curves there reported represented preliminary measurements where the conductivity values at $\phi<0.12$ differ from the data reported in the present paper due to impurity present in the measurement cell.

Coming back to the results of this paper, the formation of water channels starting from $\phi \sim 12\%$ at $T=25\,^{\circ}C$ is an indication that the system undergoes a transition from droplets to bicontinuous microemulsions at a relatively low volume fraction of the dispersed phase.

To compare the results of the sodium AOT system with those of the calcium AOT system, we have to recall that in the phase diagram of the calcium-based system [8], the maximum $[water]/[Ca(AOT)_2]$ mole ratio to observe a monophasic microemulsion behavior is ~60; this corresponds to a $[water]/[AOT^-]$ ratio of 30 [8]. In the sodium-based system, the latter is ~50 [45,46], indicating a higher ability of the microemulsion to incorporate water. Another consistent difference is the aqueous solubility of the AOT surfactant: with sodium counterion it is very high, whereas with calcium counterion the AOT is insoluble in water [8]. This leads to a minimum water to surfactant mole ratio of 4.3 to observe monophasic microemulsion samples in the

$Ca(AOT)_2$ water in *n*-decane microemulsions. If compared with the Na(AOT)-water binary system, in the $Ca(AOT)_2$-water binary system the critical micelle concentration is lower, and the lamellar phase, which is formed at high surfactant content, incorporates water to a much lower extent [47,48]. Thus, the tendency to incorporate less water is already present in the water-calcium AOT binary system. The reduction of the aqueous critical micellar concentration due to divalent counterions is well described by the Poisson-Boltzman (PB) equation, being the electrostatic free energy of a charged surface inversely proportional to the counterion valency. However, the PB equation fails to explain the micellar growth and the swelling reduction of the lamellar phase induced by divalent counterions [47–49]. Monte Carlo experiments [50] demonstrate that attractive double-layer forces appear in $Ca(AOT)_2$ lamellar phases, at high surfactant content. It has been shown that this attractive electrostatic force between lamellae does occur with divalent ions, due to the presence of image charge forces that are not present for monovalent ions [49]. The latter could be also related to the reduced ability of the calcium AOT water in *n*-decane microemulsions to incorporate water. The subject is interesting as also recently reported in [51].

We recall that SANS experiments were performed on diluted samples at 25 °C with $[water]/[Ca(AOT)_2] \sim 25$, corresponding to $[water]/[AOT^-] = 12.5$. This ratio is very close to that of the samples studied in this paper, $[water]/[Ca(AOT)_2] \sim 26.6$ ($[water]/[AOT^-] = 13.3$). By SANS [8], spherical droplets with a core radius of 21.3 Å and with polydispersity of 22% were found at $\phi < 0.10$. The corresponding sodium-based system with $[water]/[AOT^-] = 12.5$, presents droplets having an average core radius of 28 Å at 28.6 °C [17,18], which is higher than that of the calcium-based system. Furthermore, in the calcium-based microemulsions, the interfacial area for surfactant molecule was 116 $Å^2$ [8], almost twice the value found in the sodium AOT reference system [17,18,52], indicating that the calcium ion does coordinate, as expected, two $(AOT)^-$ molecules whereas sodium coordinates one. This gives support for the sodium and calcium AOT water in *n*-decane phase-diagram comparison reported above. We point out that the sodium AOT water in *n*-decane microemulsions system is composed of thermodynamically stable water droplets, coated by surfactant molecules, with a radius that increases from 25 Å to 80 Å as the water to surfactant mole ratio increases from 10 to 50 [17,18,52] and, at room temperature, no evidence of a bicontinuous structure was found in the whole L_2 region of the phase diagram.

According to this framework, the results here reported on conductivity and dielectric spectroscopy measurements indicate that the substitution of sodium with calcium ion in the studied ternary system leads to a structure that is mainly bicontinuous, except in the diluted region of the $[water]/[AOT^-] = 13.3$ line, at $\phi < 0.10$. This suggests that the packing parameter of the calcium surfactant in the interfacial region is very different from that of the sodium surfactant and that the interaction between the dispersed microdomains in the system should be also very different. The latter will be clarified by further SANS analysis of the concentrated region of the microemulsion phase diagram.

ACKNOWLEDGMENTS

The authors thank Professor S. A. Safran for a very helpful discussion. Thanks are due to M. Carlà, D. Senatra, and M. Monduzzi for helpful discussions. G. Capuzzi thanks the "Consorzio per lo sviluppo dei Sistemi a Grande Interfase, CSGI" for financial support. This work was supported by MURST, CNR, CSGI, and the INFM.

[1] J. Eastoe, G. Fragnet, B. H. Robinson, T. F. Towey, R. K. Heenan, and F. J. Leng, J. Chem. Soc., Faraday Trans. **86**, 2883 (1990).

[2] J. Eastoe, T. F. Towey, B. H. Robinson, J. Williams, and R. K. Heenan, J. Phys. Chem. **97**, 1459 (1993).

[3] R. Giordano, P. Migliardo, U. Wanderlingh, E. Bardez, and C. Vasi, J. Mol. Struct. **296**, 265 (1993).

[4] F. Aliotta, P. Migliardo, D. I. Donato, V. Turco-Liveri, E. Bardez, and B. Larrey, Prog. Colloid Polym. Sci. **89**, 258 (1992).

[5] E. Bardez, N. Cao Vy, and Th. Zemb, Langmuir **11**, 3374 (1995).

[6] R. Giordano, P. Migliardo, U. Wanderlingh, and E. Bardez, Physica B **213-214**, 585 (1995).

[7] J. Eastoe, D. C. Steytler, B. H. Robinson, R. H. Heenan, A. N. North, and J. C. Dore, J. Chem. Soc., Faraday Trans. **90**, 2479 (1994).

[8] G. Capuzzi, F. Pini, C. M. C. Gambi, M. Monduzzi, P. Baglioni, and J. Texeira, Langmuir **13**, 6927 (1997). The phase diagram herewith reported is related to the $Ca(AOT)_2$-water-normal decane system. D_2O was a typewritten error. Furthermore, the boundary line corresponding to the highest water to surfactant weight ratio was wrongly reported in the figure at 50%, instead of 55%, of surfactant over surfactant plus water.

[9] J. N. Israelachvili, in *Intermolecular & Surface Forces* (Academic Press, New York, 1992), Chap. 18.

[10] *Surfactants*, edited by Th. F. Tadros (Academic Press, London, 1984).

[11] C. Cametti, F. Codastefano, P. Tartaglia, J. Rouch, and S.-H. Chen, Phys. Rev. Lett. **64**, 1461 (1990).

[12] C. Cametti, F. Codastefano, P. Tartaglia, S.-H. Chen, and J. Rouch, Phys. Rev. A **45**, R5358 (1992).

[13] J. Rouch, L. Safouane, C. Cametti, F. Codastefano, P. Tartaglia, and S.-H. Chen, Prog. Colloid Polym. Sci. **84**, 139 (1991).

[14] F. Bordi, C. Cametti, J. Rouch, F. Sciortino, and P. Tartaglia, J. Phys.: Condens. Matter **8**, A19 (1996).

[15] J. Lang, A. Jada, and A. Malliaris, J. Phys. Chem. **92**, 1946 (1988).

[16] A. Jada, J. Lang, and R. Zana, J. Phys. Chem. **93**, 1 (1989).

[17] S.-H. Chen, Annu. Rev. Phys. Chem. **37**, 351 (1986).

[18] S.-H. Chen, T-L Lin, and J.S. Huang, in *Physics of Complex and Supramolecular Fluids*, edited by S. A. Safran and N. A.

Clark (Wiley, New York, 1987).
[19] Y. Feldman, N. Kozlovich, and N. Garti, Phys. Rev. E **51**, 478 (1995).
[20] Y. Feldman, N. Kozlovich, I. Nir, N. Garti, V. Archipov, Z. Idiyatullin, Y. Zuev, and V. Fedotov, J. Phys. Chem. **100**, 3745 (1996).
[21] N. Kozlovich, A. Puzenko, Y. Alexandrov, and Y. Feldman, Phys. Rev. E **58**, 2179 (1998).
[22] S.-H. Chen, S. L. Chang, R. Strey, J. Samseth, and K. Mortensen, J. Phys. Chem. **95**, 7427 (1991).
[23] J. Peyrelasse and C. Boned, Phys. Rev. A **41**, 938 (1990).
[24] J. Peyrelasse and C. Boned, J. Phys. Chem. **89**, 370 (1985).
[25] A. Ponton, T. K. Bose, and G. Delbos, J. Chem. Phys. **94**, 6879 (1991).
[26] M. A. van Dijk, Phys. Rev. Lett. **55**, 1003 (1985).
[27] M. A. van Dijk, G. Casteleijn, J. G. H. Joosten, and Y. K. Levine, J. Chem. Phys. **85**, 626 (1986).
[28] M. G. Giri, M. Carlà, C. M. C. Gambi, D. Senatra, A. Chittofrati, and A. Sanguineti, IEEE Trans. Dielectr. Electr. Insul. **1**, 716 (1994).
[29] M. G. Giri, M. Carà, C. M. C. Gambi, D. Senatra, A. Chittofrati, and A. Sanguineti, Phys. Rev. E **50**, 1313 (1994).
[30] C. M. C. Gambi, M. G. Giri, M. Carlà, D. Senatra, and A. Chittofrati, Phys. Rev. E **56**, 4356 (1997).
[31] S. A. Safran, I. Webman, and G. S. Grest, Phys. Rev. A **32**, 506 (1985).
[32] G. Grest, I. Webman, S. Safran, and A. Bug, Phys. Rev. A **33**, 2842 (1986).
[33] P. G. de Gennes and C. Taupin, J. Phys. Chem. **86**, 2294 (1982).
[34] U. Olsson, K. Shinoda, and B. Lindman, J. Phys. Chem. **90**, 4083 (1986).
[35] G. J. M. Koper, W. F. C. Sager, J. Smeets, and D. Bedeaux, J. Phys. Chem. **99**, 13 291 (1995).
[36] H-F. Eicke, M. Borkovec, and B. Das-Gupta, J. Phys. Chem. **93**, 314 (1989).
[37] D. G. Hall, J. Phys. Chem. **94**, 429 (1990).
[38] N. Kallay and A. Chittofrati, J. Phys. Chem. **94**, 4755 (1990).
[39] C. Boned, J. Peyrelasse, M. Clausse, B. Lagourette, J. Alliez, and L. Babin, Colloid Polym. Sci. **257**, 1073 (1979).
[40] T. Hanai, T. Imakita, and N. Koizumi, Colloid Polym. Sci. **260**, 1029 (1982).
[41] J. M. Luck, J. Phys. A **18**, 2061 (1985).
[42] M. G. Giri, M. Carlà, C. M. C. Gambi, D. Senatra, A. Chittofrati, and A. Sanguineti, Meas. Sci. Technol. **4**, 627 (1993).
[43] C. Mathew, Z. Saidi, J. Peyrelasse, and C. Boned, Phys. Rev. E **43**, 873 (1991).
[44] F. Caboi, G. Capuzzi, P. Baglioni, and M. Monduzzi, J. Phys. Chem. B **101**, 10 205 (1997).
[45] M. Kotlarchyk, S.-H. Chen, J. S. Huang, and M. W. Kim, Phys. Rev. A **29**, 2054 (1984).
[46] J. Rouviere, J.-M. Couret, M. Lindheimer, J.-L. Dejardin, and R. Marrony, J. Chim. Phys. Phys.-Chim. Biol. **76**, 289 (1979).
[47] A. Khan, K. Fontell, and B. Lindman, J. Colloid Interface Sci. **101**, 193 (1984).
[48] H. Wennerstrom, A. Khan, and B. Lindman, Adv. Colloid Interface Sci. **34**, 449 (1991).
[49] A. Khan, B. Jonsson, and H. Wennestrom, J. Phys. Chem. **89**, 5180 (1985).
[50] L. Guldbrand, B. Jonsson, H. Wennestrom, and P. Linse, J. Chem. Phys. **80**, 2221 (1984).
[51] P. A. Pincus and S. A. Safran, Europhys. Lett. **42**, 103 (1998).
[52] M. Borkovec, J. Phys. Chem. **91**, 6268 (1989).